ACS Macro Letters

Letter

pubs.acs.org/macroletters

Lithium Ion Transport Mechanism in Ternary Polymer Electrolyte-Ionic Liquid Mixtures: A Molecular Dynamics Simulation Study

Diddo Diddens*[,†,‡] and Andreas Heuer[†,‡]

[†]Institut für Physikalische Chemie, Westfälische Wilhelms-Universität, Corrensstrasse 28/30, 48149 Münster, Germany

[‡]Graduate School of Chemistry, Westfälische Wilhelms-Universität, Wilhelm-Klemm-Strasse 10, 48149 Münster, Germany

Supporting Information

ABSTRACT: The lithium transport mechanism in ternary polymer electrolytes, consisting of $PEO_{20}LiTFSI$ and various fractions of the ionic liquid $PYR_{13}TFSI$, is investigated by means of MD simulations. This is motivated by recent experimental findings (Passerini et al. *Electrochim. Acta* **2012**, *86*, 330), which demonstrated that these materials display an enhanced lithium mobility relative to their binary counterpart $PEO_{20}LiTFSI$. In order to grasp the underlying microscopic scenario giving rise to these observations, we employ an analytical, Rouse-based cation transport model (Maitra et al. *Phys. Rev. Lett.* **2007**, *98*, 227802), which has originally been devised for conventional polymer electrolytes. This model describes the cation transport via three different mechanisms, each characterized by an individual time scale. It turns out that also in the ternary electrolytes essentially all lithium ions are coordinated by PEO chains, thus, ruling out a transport mechanism enhanced by the presence of ionic-liquid molecules. Rather, the plasticizing effect of the ionic liquid contributes to the increased lithium mobility by enhancing the dynamics of the PEO chains and consequently also the motion of the attached ions. Additional focus is laid on the prediction of lithium diffusion coefficients from the simulation data for various chain lengths and the comparison with experimental data, thus demonstrating the broad applicability of our approach.

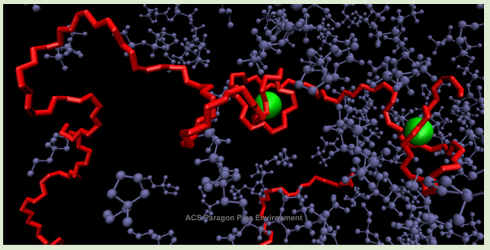

Solid polymer electrolytes (SPEs) are promising candidates for lithium ion batteries, as they are ideal to create small and light-weight but powerful energy storages.[1,2] The classical SPEs consist of an amorphous polymer matrix, e. g. poly(ethylene oxide) (PEO), and a lithium salt dissolved in it.[3,4] By using lithium salts with large anions such as lithium-bis(trifluoromethane)sulfonimide (LiTFSI), the crystallization can be suppressed as the negative charge is delocalized over the whole anion. However, at ambient temperatures, the conductivity of most SPEs is still too low for an efficient technological use. Among several other remedies,[5−8] the incorporation of a room temperature ionic liquid (IL) seems to be a very promising approach,[9,10] as the resulting ternary electrolytes show both an increased conductivity and inherent stability. Moreover, ILs are nonvolatile, nonflammable,[11] and exhibit a wide electrochemical stability window.[12]

However, it is not yet fully understood how far the lithium transport mechanism in these materials changes relative to the conventional polymer electrolytes. For instance, it was speculated[9] that the lithium ions become progressively coordinated by the anions from the IL and are thus decoupled from the rather slow PEO chains. Alternatively, one might also expect that the IL enhances the PEO dynamics and serves as a plasticizer in this way, which is a common observation when adding low-molecular solvents to PEO-salt systems.[6−8] In this work, we utilize molecular dynamics (MD) simulations to unravel the impact of the addition of IL. In order to quantify the lithium motion, we employ an analytical cation transport model,[13,14] which has originally been devised for binary polymer electrolytes.

Our description is based on both the Rouse model[15] as well as the dynamic bond percolation (DBP) model[16] and distinguishes three different microscopic lithium ion transport mechanisms (Figure 1): (1) The ions diffuse along the PEO backbone to which they are attached. This motion can be characterized by the time scale τ_1 the ions need to explore the entire PEO chain. (2) For ambient temperatures, the PEO chains are naturally also subject to thermal motion, carrying the attached ions in this way. In case of Rousean motion, the polymer dynamics and, thus, the motion of the attached ions can be quantified by an effective Rouse time τ_2. (3) Finally, an

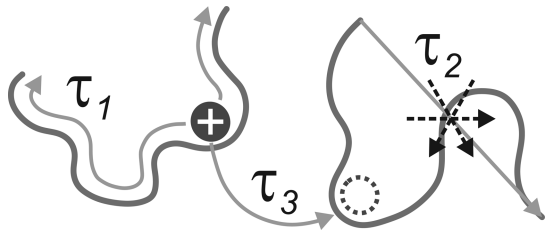

Figure 1. Scheme illustrating the three cation transport mechanisms in PEO-salt electrolytes.

Received: December 15, 2012
Accepted: March 18, 2013
Published: April 2, 2013

ion bound to a specific PEO chain can be transferred to another chain. The mean residence time at a given chain is denoted as τ_3 in the following. As demonstrated earlier,[13] the last mechanism can also be viewed as a renewal process within the framework of the DBP model.

Of course, for the ternary electrolytes, it is a priori unclear if this scenario changes only quantitatively, reflected by different values for τ_1, τ_2, and τ_3, or if the lithium ion transport mechanism also changes on a qualitative level. In particular, we focus on two ternary polymer electrolytes with the same IL as in ref 9, that is, *N*-methyl-*N*-propylpyrrolidinium TFSI ($PYR_{13}TFSI$), with a stoichiometry of $PEO_{20}LiTFSI{\cdot}0.66PYR_{13}TFSI$ and $PEO_{20}LiTFSI{\cdot}3.24PYR_{13}TFSI$, respectively. The binary polymer electrolyte, $PEO_{20}LiTFSI$, serves as a reference. For convenience, PEO will be abbreviated as "P" and LiTFSI as "S" in the following, leading to the short-hand notation $P_{20}S{\cdot}x$IL with x = 0, 0.66, and 3.24.

The simulations were performed with the AMBER 10 package.[17] Here, the sander module was modified, allowing us to use a many-body polarizable force field specifically designed for PEO/LiTFSI[18,19] and $PYR_{13}TFSI$.[20] The simulation box contained 10 PEO chains with N = 54 monomers each as well as 27 LiTFSI ion pairs, yielding a concentration of ether oxygens (EOs) to lithium ions of 20:1. Additionally, the two ternary systems contained 18 or 87 $PYR_{13}TFSI$ molecules, corresponding to x = 0.66 and x = 3.24. The simulation cells have been created randomly in the gas phase to yield homogeneous systems. After equilibration runs of 70−80 ns in the *NpT* ensemble, production runs with a length of 200 ns have been performed in the *NVT* ensemble, collecting data every picosecond. An elementary integration step of 1 fs was used, while the systems were coupled to a Berendsen thermostat[21] with a reference temperature of 423 K. All bonds involving hydrogen were constrained by the SHAKE algorithm.[22] The induceable point dipoles were integrated by a Car−Parrinello-like scheme.[23] By comparing various radial distribution functions and mean square displacements (MSDs) for the first and the second half of the runs, we confirmed that the systems are in equilibrium. Moreover, the former showed no long-range ordering, demonstrating that the systems are perfectly mixed.

We find for all electrolytes that virtually all lithium ions are coordinated to one or two PEO chains, thereby giving a first hint that also for the ternary systems the cation transport entirely takes place at the PEO chains. Details of the Li^+ coordination and the polymer structure are discussed in section 1 of the Supporting Information (SI).

Although from a structural point of view no significant differences emerge upon the addition of IL (see SI), we observe a clear increase of the lithium MSD with increasing x, especially for the subdiffusive regime at t = 1−10 ns (crosses in Figure 2), whereas the onset to diffusion occurs on comparable time scales, that is, t = 20−50 ns. A similar increase can be found for the MSD of the entire PEO chains (inset of Figure 2). In the following, we will go more into detail and investigate the relative importance of the individual transport mechanisms.

To calculate the renewal times, the number of transfer processes N_{tr} was counted from the simulations, and the τ_3-values were determined according to $\tau_3 = t_{max}N^+_{Li}/N_{tr}$, where t_{max} = 200 ns is the simulation length and N^+_{Li} = 27 is the number of lithium ions in the simulation box. Of course, it is questionable if brief transfers followed by successive backjumps to the previous polymer chain serve as a renewal process in the

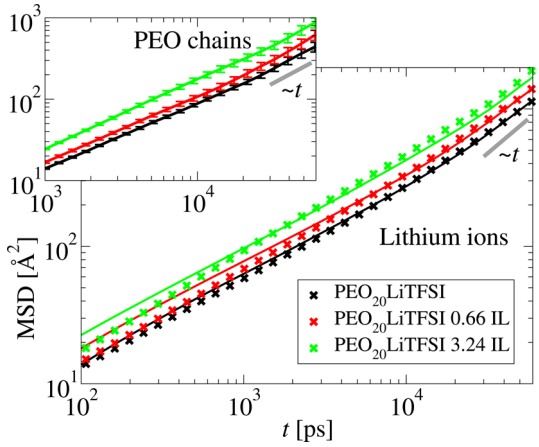

Figure 2. MSD of the lithium ions (main panel) and the center of mass of the PEO chains (inset). The solid lines in the main panel correspond to the model predictions.

strict sense, because the lithium dynamics will not become uncorrelated to its past after such an event. A more detailed analysis (not shown) revealed that these non-Markovian, short-time backjumps occurred up to 100 ps, which we used subsequently as a criterion to define real renewal events. In cases where the transfer was mediated by TFSI anions only (probability p_{IL} in Table 1), we found that the displacement the ion covers in the IL-rich region was sufficiently small, so that the contribution of these transfers to the lithium MSD is negligible.

We observe that τ_3 (Table 1) increases with increasing IL concentration. Because the PEO molecules become more and more diluted, this can mainly be explained as a concentration effect. Obviously, the critical step for a transfer process is the encounter of a another PEO segment.

To quantify the diffusion along the PEO backbone, we successively numbered all monomers at a given PEO chain, allowing us to express the lithium position by the average ether oxygen (EO) index n and to calculate an effective MSD $\langle\Delta n^2(t)\rangle$ along this coordinate (see SI, section 2). We find that this type of motion is slightly subdiffusive (i.e., $\langle\Delta n^2(t)\rangle \propto t^{0.8}$) for all electrolytes within the statistical error. No significant dependence on the IL concentration can be observed. This indicates that the surrounding molecules (PEO chains or IL) have no influence on this mechanism. To estimate the net effect of this mechanism (i.e., the number of traversed monomers before the ion is transferred to another chain), we define τ_1 via[13]

$$\tau_1 = \frac{(N-1)^2}{\pi^2}\frac{2\tau_3}{\langle\Delta n^2(\tau_3)\rangle} \quad (1)$$

which due to the subdiffusivity of $\langle\Delta n^2(t)\rangle$ slightly depends on τ_3 (Table 1, see SI for calculational details). One observes that τ_1 decreases slightly with increasing IL concentration, reflecting the weak dependence of τ_1 on τ_3.

Figure 3 shows the MSD of the EOs relative to the center of mass of the PEO chain. This quantity has been computed for all EOs (i.e., irrespective of the presence of an ion) and for EOs bound to a lithium ion, as well as for the respective attached ions. The criterion to consider a cation or EO as bound was that the average EO index of the ion did not change more than one, that is, $|\Delta n(t)| \leq 1$ for all time frames during t. For the bound EOs, no further distinction between additional

dx.doi.org/10.1021/mz3006457 | ACS Macro Lett. 2013, 2, 322−326

Table 1. Parameters Characterizing the Three Transport Mechanisms (see Text for Further Explanation)

x_{IL}	τ_1 (ns)	$\langle R_e^2\rangle$ (Å^2)	τ_R (ns)	τ_2 (ns)	τ_3 (ns)	p_{IL} (%)	D_{Li}^{sim} (Å^2 ns^{-1})	D_{Li}^{∞} (Å^2 ns^{-1})	D_{Li}^{exp} (Å^2 ns^{-1})[10]
0.0	147	1662	45	167	17	2.5	2.945	1.947	0.052 (x = 0.0)
0.66	140	1570	37	89	18	1.0	3.542	2.309	0.118 (x = 1.0)
3.24	127	1571	24	68	24	8.5	4.257	2.392	0.126 (x = 4.0)

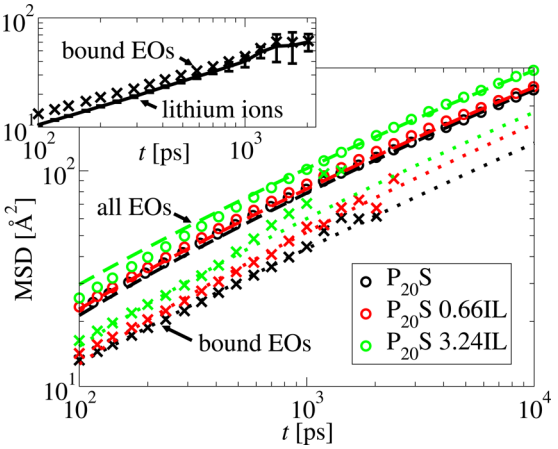

Figure 3. MSDs of the average EOs (circles), the bound EOs (crosses) and the lithium ions bound to these EOs (inset, solid lines). The dashed and dotted lines show the respective Rouse fits.

coordinations of the lithium ion to another PEO chain or a TFSI molecule was made. Thus, these effects are already implicitly contained in the curves in Figure 3. Of course, it is questionable if cations bound to two PEO chains show the same dynamics as ions bound to one chain only, because the former could be regarded as transient cross-links, which would significantly impede the polymer motion. A more detailed analysis indeed revealed that there is a conceptual difference between these two coordinations, however, this effect can easily be taken into account (see SI, section 3) and does not affect the general formalism of our analysis.

The average EOs (circles) show typical Rouse-like motion with the characteristic relaxation time τ_R. The dynamics of the bound EOs (crosses) is qualitatively the same but protracted. Therefore, it is possible to characterize the dynamics of the bound EOs by a larger, effective Rouse time τ_2. The lithium ions attached to these EOs (shown in the inset of Figure 3 for $P_{20}S$, the curves for the other electrolytes look similar) closely follow the bound EOs, which gives clear evidence for their cooperative motion. On short time scales, the MSD of the EOs is larger than the lithium MSD due to the additional internal degrees of freedom of the PEO backbone, but the MSD of the bound cations catches up at $t \approx 1$ ns. Thus, τ_2 characterizes both the dynamics of the bound PEO segments as well as of the attached lithium ions.

Figure 3 also shows the Rouse fits, that is, $g_R(t) = 2\langle \mathbf{R}_e^2\rangle \pi^{-2} \sum_{p=1}^{N-1} [1 - \exp(-tp^2/\tau_R)] p^{-2}$, for the average (dashed lines) and for the bound EOs (dotted lines). Of course, the precise value of τ_R and τ_2 also depends on the value of $\langle \mathbf{R}_e^2\rangle$. To obtain a fit consistent with the plateau value at large t (not shown in Figure 3 for clarity), the MSDs of the average EOs were fitted using two parameters, that is, τ_R and $\langle \mathbf{R}_e^2\rangle$. Subsequently, the MSDs of the bound EOs were fitted using this value in combination with a single fit parameter τ_2 only (Table 1, deviations from our previous study[14] on $P_{20}S$ arise from the shorter simulation length of about 27 ns and the modified fitting procedure).

Whereas the $\langle \mathbf{R}_e^2\rangle$-values are approximately constant, both τ_R and τ_2 decrease significantly, clearly indicating that the dynamics of the PEO segments becomes faster with increasing IL concentration. Therefore, the IL can be regarded as plasticizer. For the average segments, the dynamics for $P_{20}S{\cdot}3.24$IL is nearly the same as for pure PEO (τ_R = 22 ns), showing that the plasticizing approximately cancels with the slowing-down caused by the coordinating lithium ions as found for $P_{20}S$. The presence of the IL also enhances the motion of the bound segments, and, as a result, the dynamics of the respective attached lithium ions, leading to an increase of the overall lithium MSD. Here, experimental studies reported similar findings for other plasticizers like ethylene/propylene carbonate[7,8] or short PEO chains embedded in a high molecular weight matrix.[6,8]

For finite N, the plasticizing effect is even 2-fold. Apart from the internal, segmental PEO dynamics (Figure 3), the center-of-mass motion is also accelerated by the addition of IL (inset of Figure 2). The relative importance of these two types of plasticizing will be discussed below.

As a consistency check of our description, we employ the transport model to reproduce the lithium MSD in Figure 2. During the residence time $\tilde{t}$ at a given PEO chain, the MSD g_{12} of the lithium ion is given by a Rouse-like expression[13]

$$g_{12}(\tilde{t}) = \frac{2\langle \mathbf{R}_e^2\rangle}{\pi^2} \sum_{p=1}^{N-1} \frac{\left[1 - \exp\left(\frac{-\tilde{t}p^2}{\tau_{12}}\right)\right]}{p^2} \qquad (2)$$

where $\tau_{12}^{-1} = \tau_1^{-1} + \tau_2^{-1}$ is a combined relaxation rate due to both intramolecular mechanisms. After a renewal process (i.e., an interchain transfer), the ion dynamics becomes uncorrelated to its past,[13,16] and the motion at the new chain is again characterized by eq 2. Thus, it is possible to interpret the overall lithium dynamics as a random walk, in which the elementary step length is given by eq 2, and the direction of motion for the successive step changes randomly after each renewal event. We assumed that the number of ion transfer processes during time interval t is given by a Poisson distribution with mean t/τ_3, leading to exponentially distributed $\tilde{t}$. For a given t, the lithium MSD due to the three transport mechanisms was then obtained from the numerical average over a large number of Poisson processes. The third ingredient required for the total lithium MSD is the center-of-mass motion of the PEO chains, which was directly extracted from the simulations (inset of Figure 2) and added to the model curve. The resulting predictions are shown as solid lines in the main panel of Figure 2, the respective diffusion coefficients D_{Li}^{sim} calculated from the model curves are given in Table 1.

For $P_{20}S$, one observes a nearly perfect agreement throughout the entire observation time. This demonstrates that our transport model indeed captures the underlying, much more complex microscopic scenario. In the case of $P_{20}S{\cdot}0.66$IL and $P_{20}S{\cdot}3.24$IL, the model curves agree with the empirical

dx.doi.org/10.1021/mz3006457 | ACS Macro Lett. 2013, 2, 322−326

lithium MSD for time scales larger than about 1−2 ns. Slight deviations can be attributed to the large uncertainties of the MSD of the PEO chains. However, the model prediction systematically overestimates the MSDs of $P_{20}S{\cdot}0.66IL$ and $P_{20}S{\cdot}3.24IL$ for short time scales. Here, a more detailed analysis (to be published under separate cover) revealed that these deviations are caused by hydrodynamic interactions arising from the presence of the IL. On larger length and time scales, these hydrodynamic interactions are screened, which has also been reported for other semidilute polymer solutions.[24] Thus, both the Rouse-like behavior and the diffusive regime are correctly reproduced, which clearly demonstrates the applicability of our model to the experimentally relevant long-time limit.

Finally, we use the same procedure as above to compute D_{Li}^{∞} for $N \to \infty$ via the scaling laws[13] $\langle \mathbf{R}_e^2 \rangle \propto N$, $\tau_1 \propto N^2$, $\tau_2 \propto N^2$, and $\tau_3 \propto N^0$. Of course, for the scaling of τ_2, entanglement effects may become relevant, which would slow down the segmental dynamics. However, if $\tau_3 < \tau_e$ (i.e., the entanglement time), meaning that the lithium ion leaves the PEO chain before the latter begins to reptate, the overall dynamics is still Rousean,[25] and our model can still be used to calculate D_{Li}. For PEO, experiments[26] revealed that the entanglement regime sets in from about $N \approx 75$. Based on these observations, one can estimate τ_e according to $\tau_e = \tau_R(N = 75) = \tau_R(75/54)^2$. For $P_{20}S$, this leads to $\tau_e \approx 87$ ns, which is substantially larger than τ_3. Also, in case of the highly plasticized $P_{20}S{\cdot}3.24IL$, one finds $\tau_e \approx 46$ ns $> \tau_3$. Therefore, the lithium ion leaves the PEO chain before the tube constraints become noticeable, and our formalism can also be applied for $N \to \infty$.

Table 1 shows D_{Li}^{∞} calculated from the model together with the PFG-NMR data[10] at $T = 323$ K. For the experimental measurements, both the IL fraction x and the IL cation, that is, PYR_{14}, are slightly different than in our simulations, however, one would expect no significant effect on the transport mechanism. In both cases, we observe a clear increase of D_{Li}, which can be attributed to the plasticizing effect of the IL.

However, when discussing these values, one has to keep in mind that, not only the segmental motion, but also τ_3 and D_{PEO} affect the precise value of D_{Li}, in which each contribution has its own N-dependence. For example, in the case of $N \to \infty$, the mean intramolecular MSD $\langle g_{12} \rangle$ (averaged over all $\tilde{t}$, eq 2), increases by about 28% for $P_{20}S{\cdot}0.66IL$ and 73% for $P_{20}S{\cdot}3.24IL$, mainly as a result of the increased segmental mobility. On the other hand, the renewal rate decreases by about 7 and 29%, although the plasticizing effect dominates, and the overall D_{Li}^{∞}-values increase by about 19 and 23%. For $N = 54$, the situation is slightly different. Here, the segmental plasticizing, measured by $\langle g_{12} \rangle$, leads only to an increase of 22% for $x = 0.66$ and 54% for $x = 3.24$. Finally, for $N \to 1$, the differences in $\langle g_{12} \rangle$ would even disappear.[13] However, this trend is compensated by the plasticizing of the center-of-mass motion of PEO. For $N = 54$, D_{PEO} is raised by 30% for $x = 0.66$ and by 92% for $x = 3.24$, which results in an overall increase of D_{Li} of 20% for $P_{20}S{\cdot}0.66IL$ and 45% for $P_{20}S{\cdot}3.24IL$.

So far, we focused on the high-temperature limit which we can address in our simulations. Interestingly, the relative increase of D_{Li}^{exp} upon the addition of IL becomes much more pronounced in the low-temperature regime[10] (see also Table 1). Although simulations at low temperatures would be too costly, one might expect that the plasticizing effect at least partly accounts for the larger relative increase of D_{Li} in this regime. Here, DSC measurements[10] revealed that the glass-transition temperature decreases up to 35 K upon IL addition, which gives a first hint that, also at low temperatures, the enhanced polymer dynamics contributes to the faster lithium motion. In such a scenario, the plasticizing of the polymer matrix via electrochemically stable additives would be an important milestone for the use of SPE-based batteries in electronic devices, as their current limitation particularly holds for low (i.e., ambient) temperatures. In fact, PEO/LiTFSI/IL mixtures have recently been successfully applied in prototype batteries.[27]

In this study, we have examined the microscopic lithium ion transport mechanism in ternary polymer electrolytes consisting of $PEO_{20}LiTFSI$ and $PYR_{13}TFSI$. In particular, we addressed the question in how far the microscopic scenario of the ion transport changes upon the addition of IL and how the experimentally observed increase in the lithium ion diffusion coefficient[10] can be understood in terms of the individual transport mechanisms. To this purpose, an analytical cation transport model[13] was successfully applied. It turned out that virtually all lithium ions were coordinated to the PEO chains, thus ruling out a transport mechanism in which the lithium transportation is decoupled from the polymer chains. Rather, the main reason for the increase of the lithium diffusion coefficient, at least for the considered temperature, is the plasticizing effect of the IL, which enhances the segmental motion of the PEO chains and thus also the dynamics of the attached ions. A minor counteracting effect was the successive dilution of the electrolyte due to the IL, which slightly decreases the rate of interchain transfers. In the sum, however, the plasticizing is dominant, and the overall lithium diffusivity increases. For the design of novel battery materials, our findings therefore imply that a polymer electrolyte which is both highly plasticized and exhibits a high transfer rate, for example, facilitated by a more coordinating IL, would yield optimal results.

■ ASSOCIATED CONTENT

Supporting Information

Supplementary analyses: discussion of the structural properties, characterization of the diffusion along the PEO chain, and evaluation in how far the lithium ions act as temporary cross-links. This material is available free of charge via the Internet at http://pubs.acs.org.

■ AUTHOR INFORMATION

Corresponding Author

*E-mail: d.diddens@uni-muenster.de.

Notes

The authors declare no competing financial interest.

■ ACKNOWLEDGMENTS

The authors would like to thank Oleg Borodin, Nicolaas A. Stolwijk, Stefano Passerini, and Mario Joost for helpful discussions and for providing the experimental data. Financial support from the NRW Graduate School of Chemistry is also greatly appreciated.

■ REFERENCES

(1) Gray, F. M. *Solid Polymer Electrolytes*; Wiley-VCH: New York, 1991.

(2) Bruce, P. G.; Vincent, C. A. *J. Chem. Soc., Faraday Trans.* **1993**, *89*, 3187−3203.

(3) Fenton, D. E.; Parker, J. M.; Wright, P. V. *Polymer* **1973**, *14*, 589.

(4) Armand, M. B. Ann. *Rev. Mater. Sci.* **1986**, *16*, 245−261.
(5) Gang, W.; Roos, J.; Brinkmann, D.; Capuano, F.; Croce, F.; Scrosati, B. *Solid State Ionics* **1992**, *53*, 1102−1105.
(6) Borghini, M. C.; Mastragostino, M.; Zanelli, A. *Electrochim. Acta* **1996**, *41*, 2369−2373.
(7) Bandara, L. R. A. K.; Dissanayake, M. A. K. L.; Mellander, B. E. *Electrochim. Acta* **1998**, *43*, 1447−1451.
(8) Kim, Y. T.; Smotkin, E. S. *Solid State Ionics* **2002**, *149*, 29−37.
(9) Shin, J. H.; Henderson, W. A.; Passerini, S. *Electrochem. Commun.* **2003**, *5*, 1016−1020.
(10) Joost, M.; Kunze, M.; Jeong, S.; Schönhoff, M.; Winter, M.; Passerini, S. *Electrochim. Acta* **2012**, *86*, 330−338.
(11) Adam, D. *Nature* **2000**, *407*, 938−940.
(12) MacFarlane, D. R.; Huang, J. H.; Forsyth, M. *Nature* **1999**, *402*, 792−794.
(13) Maitra, A.; Heuer, A. *Phys. Rev. Lett.* **2007**, *98*, 227802.
(14) Diddens, D.; Heuer, A.; Borodin, O. *Macromolecules* **2010**, *43*, 2028−2036.
(15) Rouse, P. E. *J. Chem. Phys.* **1953**, *21*, 1272−1280.
(16) Nitzan, A.; Ratner, M. A. *J. Phys. Chem.* **1994**, *98*, 1765−1775.
(17) Case, D. A. et al. *Amber 10*; University of California: San Francisco, 2008.
(18) Borodin, O.; Smith, G. D. *J. Phys. Chem. B* **2006**, *110*, 6279−6292.
(19) Borodin, O.; Smith, G. D. *J. Phys. Chem. B* **2006**, *110*, 6293−6299.
(20) Borodin, O.; Smith, G. D. *J. Phys. Chem. B* **2006**, *110*, 11481−11490.
(21) Berendsen, H. J. C.; Postma, J. P. M.; van Gunsteren, W. F.; DiNola, A.; Haak, J. R. *J. Chem. Phys.* **1984**, *81*, 3684−3690.
(22) Ryckaert, J. P.; Ciccotti, G.; Berendsen, H. J. C. *J. Comput. Phys.* **1977**, *23*, 327−341.
(23) van Belle, D.; Froeyen, M.; Lippens, G.; Wodak, S. J. *Mol. Phys.* **1992**, *77*, 239−255.
(24) Ahlrichs, P.; Everaers, R.; Dünweg, B. *Phys. Rev. E* **2001**, 64.
(25) Doi, M.; Edwards, S. F. *The Theory of Polymer Dynamics*; Oxford Science Publications: Clarendon, Oxford, 2003.
(26) Shi, J.; Vincent, C. A. *Solid State Ionics* **1993**, *60*, 11−17.
(27) Balducci, A.; Jeong, S. S.; Kim, G. T.; Passerini, S.; Winter, M.; Schmuck, M.; Appetecchi, G. B.; Marcilla, R.; Mecerreyes, D.; Barsukov, V.; Khomenko, V.; Cantero, I.; De Meatza, I.; Holzapfel, M.; Tran, N. *J. Power Sources* **2011**, *196*, 9719−9730.